SPECTROSCOPIC APPLICATIONS USING RING-DOWN CAVITIES

Giel Berden
FOM Institute for Plasma Physics
Edisonbaan 14, 3439 MN Nieuwegein, The Netherlands

Gerard Meijer
FOM Institute for Plasma Physics Rijnhuizen
Edisonbaan 14, 3439 MN Nieuwegein, The Netherlands, and
Department of Molecular and Laser Physics, University of Nijmegen
Toernooiveld 1, 6525 ED Nijmegen, The Netherlands

Wim Ubachs
Laser Centre, Department of Physics and Astronomy, Vrije Universiteit,
De Boelelaan 1081, 1081 HV Amsterdam, The Netherlands

Chapter 2, pages 47-82

in

Experimental methods in Physical Sciences Volume 40
Cavity Enhanced Spectroscopies
van Zee & Looney (Editors)

2 SPECTROSCOPIC APPLICATIONS USING RING-DOWN CAVITIES

Giel Berden
FOM Institute for Plasma Physics
Edisonbaan 14, 3439 MN Nieuwegein, The Netherlands

Gerard Meijer
FOM Institute for Plasma Physics Rijnhuizen
Edisonbaan 14, 3439 MN Nieuwegein, The Netherlands, and
Department of Molecular and Laser Physics, University of Nijmegen
Toernooiveld 1, 6525 ED Nijmegen, The Netherlands

Wim Ubachs
Laser Centre, Department of Physics and Astronomy, Vrije Universiteit,
De Boelelaan 1081, 1081 HV Amsterdam, The Netherlands

2.1 Introduction

The present chapter deals with the applications of cavity ring-down spectroscopy and its variants. In a first section, a rather large number of studies involving the weak transitions in the oxygen molecule, including the effects of magnetic fields and collisions, are described. This molecule has served as a benchmark system to demonstrate the opportunities of ring-down techniques. In a subsequent section, we give an overview of the studies in which ring-down techniques have been applied to produce new spectroscopic data on molecules. In the last section, we have listed some pros and cons of ring-down techniques and the alternative techniques commonly used in molecular spectroscopy: laser-induced fluorescence, resonantly enhanced multi-photon ionization, coherent anti-Stokes Raman spectroscopy, degenerate four-wave-mixing and the non-laser Fourier-transform spectroscopic technique.

2.2 O_2: A Benchmark System for Ring-down Techniques

In many studies performed to demonstrate aspects of Ring-down techniques the oxygen molecule is chosen as the target; this choice is connected to the properties of a somewhat peculiar set of low-lying electronic states in this molecule. Its lowest molecular orbital configuration $(1s\sigma_g)^2(1s\sigma_u^*)^2(2s\sigma_g)^2(2s\sigma_u^*)^2(2p\sigma_g)^2(2p\pi_u)^4(2p\pi_g^*)^2$ gives rise to the three well-known lowest electronic states of the molecule: the electronic ground state $X^3\Sigma_g^-$ and the excited states $a^1\Delta_g$ and $b^1\Sigma_g^+$. Transitions between the ground state and these excited states are well-studied: the $b^1\Sigma_g^+$ - $X^3\Sigma_g^-$ transition, in the visible range is called the Atmospheric system, while the $a^1\Delta_g$ - $X^3\Sigma_g^-$ transition is called the Infrared atmospheric

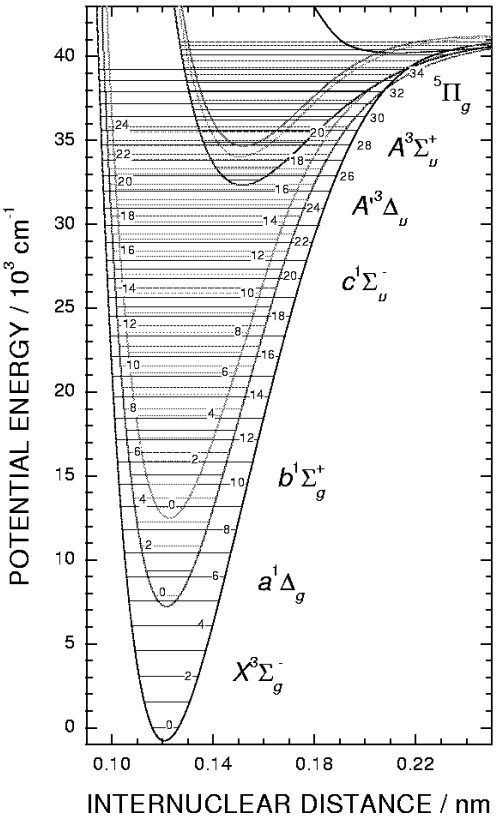

Figure 1: Potential energy curves and vibrational energies of the important low-lying electronic states correlating with $O(^3P)+O(^3P)$ dissociation limits. Figure kindly provided by Dr. R. Copeland of SRI International, Menlo Park, USA.

system. Also known is the Noxon ($b^1\Sigma_g^+$ - $a^1\Delta_g$) system connecting the two electronically excited states. As shown in Fig. 1 besides these states there are more bound states correlating with two ground state oxygen atoms $O(^3P)+O(^3P)$: the $c^1\Sigma_u^-$, $A'^3\Delta_u$, and $A^3\Sigma_u^+$ state. The three systems connecting the electronic ground state to these states, observed in the ultraviolet, $A^3\Sigma_u^+$ - $X^3\Sigma_g^-$, $A'^3\Delta_u$ - $X^3\Sigma_g^-$, and $c^1\Sigma_u^-$ - $X^3\Sigma_g^-$, are referred to as the Herzberg I, II and III systems. The lowest excited state, $a^1\Delta_g$, is connected to these three excited states as well, but only the Chamberlain bands ($A'^3\Delta_u$ - $a^1\Delta_g$) and the Richard-Johnson system ($c^1\Sigma_u^-$ - $a^1\Delta_g$) were experimentally observed. As follows from an *ab initio* study of the low-lying states of O_2 apart from the six observed bound states there are a number of additional states, $^3\Pi_u$, $^1\Pi_g$, $^5\Pi_u$, $^5\Sigma_u^-$ and $^5\Pi_g$ all correlating with $O(^3P)+O(^3P)$; these states are basically repulsive at the first few Å of internuclear separation and all very weakly bound at large internuclear separation [1]. The $^5\Pi_g$ state, with the largest well-depth of the quintet states (0.16 eV), is included in Fig. 1.

Between the lowest six of these states 15 radiative transitions are conceivable, but the peculiarity lies in the fact that they are all forbidden in the electric dipole approximation. Hence the electronic transitions are very weak and only eight of them have been observed. The excited state lifetime of the $b^1\Sigma_g^+$ state is about 11 s; the transition, connecting to the ground state, is threefold forbidden in view of Σ^+ - Σ^-, triplet-singlet, and $g-g$ transitions. The $b-X$ system, allowed for magnetic dipole transitions, is a factor of 10^9 weaker than typical electric dipole allowed transitions. The higher lying $v > 0$ vibrational levels in the $b^1\Sigma_g^+$ state suffer from much lower Franck-Condon overlap with the $X^3\Sigma_g^-$, $v = 0$ ground state level, resulting in oscillator strengths of $f_{10} = 1.6 \times 10^{-11}$ and $f_{20} = 6.3 \times 10^{-13}$. Nevertheless it were these two weak transitions, the Atmospheric B and γ bands, that were recorded in the first experiment demonstrating Cavity-Ring Down (CRD) spectroscopy [2]. Particularly because of the weakness of the bands, and in view of the easy availability of oxygen gas and the atmospheric transitions being in the range of commercially available tunable lasers, these transitions have served as the prototypical test systems in many subsequent studies, demonstrating the power and sensitivity of Ring-down techniques. In fact before the invention of the powerful CRD-method, some physically related techniques using the enhancement properties of cavities, also focused on the forbidden optical transitions of the oxygen molecule to demonstrate their power and feasibility [3, 4].

2.2.1 The $b^1\Sigma_g^+$- $X^3\Sigma_g^-$ Atmospheric System

Naus and Ubachs and co-workers have measured the CRD absorption spectra of the $b^1\Sigma_g^+$-$X^3\Sigma_g^-(v,0)$ bands ($v = 0-3$) of $^{16}O_2$, $^{16}O^{18}O$, $^{16}O^{17}O$, $^{18}O_2$, $^{17}O^{18}O$, and $^{17}O_2$ isotopomers of oxygen [5, 6, 7, 8]. In these works the focus was on spectroscopy and the generic pulsed cavity-ring down technique, with a fitting of the decay transients. As a result new or improved molecular constants for the $b^1\Sigma_g^+, v$ states were determined for all isotopomers, while for $^{17}O_2$ the constants in the $X^1\Sigma_g^+, v = 0$ ground state were determined. Note that the (3,0) band near 590 nm, also referred to as the δ-band is 10^4 times weaker than the (0,0) band; part of a recorded spectrum for the δ-band of $^{16}O_2$ at a pressure of 183 torr of natural oxygen is shown in Fig. 2. The same δ-band was also investigated by means of IntraCavity Laser Absorption Spectroscopy (ICLAS) [9] and this allows for a comparison of this method with the pulsed laser cavity-ring down technique; the ICLAS spectrum yielded a similar signal-to-noise ratio (SNR), but was recorded at 3.5 times higher pressure, resulting also in somewhat collisionally broadened lines. The SNR in the generic CRD-experiment depends of course strongly on the reflectivity of the mirrors used, and this was $R > 99.99\%$ in Ref. [8].

The CRD-studies of Refs. [5, 6, 7, 8] focused on an improvement of the spectroscopy of the $b-X$ system of O_2, in particular for the less abundant isotopomers. In view of the inherent Doppler broadening of the CRD-technique the accuracy in the old work of Babcock and Herzberg [10] could not be significantly improved. In fact also the sensitivity, previously obtained from long atmospheric path lengths, is comparable to that of the recent CRD-studies; some lines of the weakest δ-band were already recorded back in 1948. In Ref. [5],

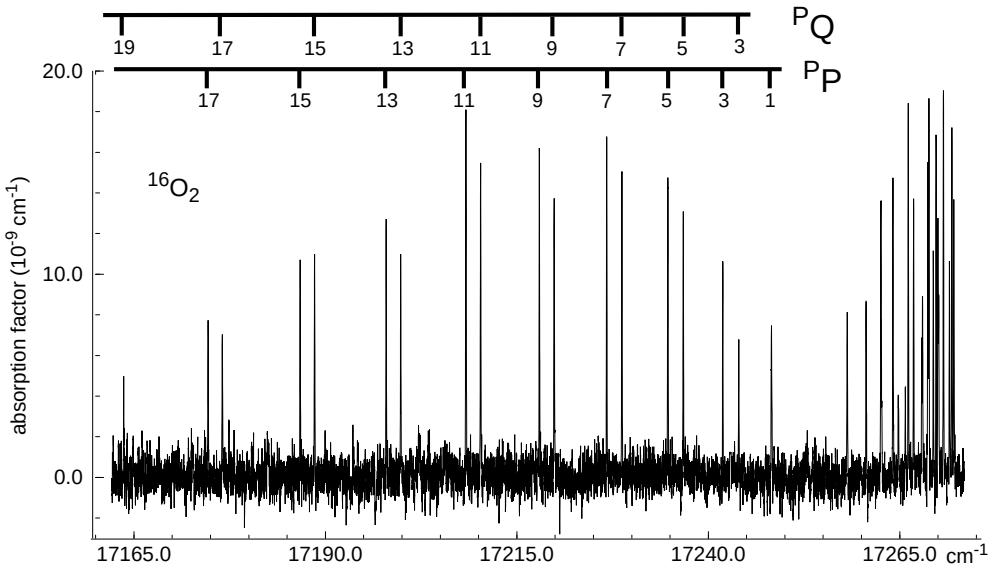

Figure 2: Cavity-ring down spectral recording of the $b - X(3,0)$ band of $^{16}O_2$ at a pressure of 183 torr. The baseline was corrected for the loss rate related to the mirror reflectivity. For the P-branches an assignment is given. Reproduced with permission from Ref. [8].

using pulsed CRD near 760 nm with mirrors of $R \approx 99.998\%$, a quadrupole transition in the $b - X(0,0)$ band, with an intensity of $2{\times}10^{-9}$ cm^{-1} could be observed, demonstrating the high sensitivity. It is noted, however, that such transitions were observed, even with higher SNR, from atmospheric absorption measurements over 43-atm km absorption path lengths [11].

In the pulsed CRD-experiments some of the isotopic species were observed in natural abundance, as previously in atmospheric absorption, but also isotopically enriched samples could be used. This demonstrates a notable advantage of the ring-down setup: long effective path lengths, and therewith high spectroscopic sensitivity can be obtained from small cavities for which only minute gas samples are required. Here the CRD-technique is favored over the alternative application of FT-spectrometers attached to White-multipass-cells, where much higher gas inputs are required. Particularly when applied to expensive isotopically enriched gas samples this advantage is of importance. With the use of a cell of 40 cm length, a diameter of 1 cm and a pressure of 180 torr, a spectrum of the very weak δ-band of $^{18}O_2$ could be recorded [8] from a sample of ≈ 10 atm cm^3 or 4×10^{-4} molar. Similarly, in an application of phase-shift CRD the γ-band of $^{18}O_2$ was measured using a minute sample cell [12].

Also the use of the Cavity-Enhanced Absorption (CEA)-variant of Ring-down techniques (discussed below) in application to an absorption measurement of oxygen in a slit jet demonstrates a specific advantage over FT-techniques. The $^PP_1(1)$ line of the $b^1\Sigma_g^+$-$X^3\Sigma_g^-(0,0)$ band of $^{16}O_2$ could be measured with a cavity of only 10-cm length [13]. The

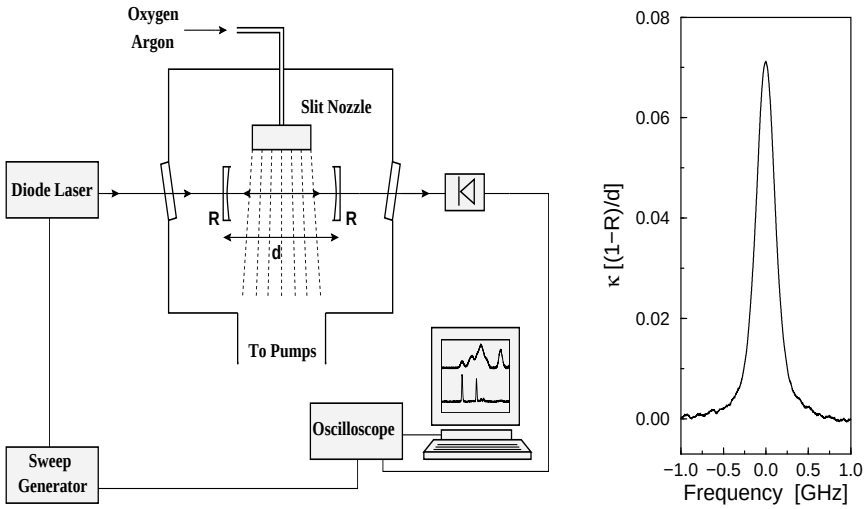

Figure 3: Left: Scheme of the experimental set-up (Ref. [13]); Right: CEA spectrum of the ${}^{P}P_1(1)$ transition of the A band of ${}^{16}O_2$ measured in a 10 cm long optical cavity positioned around a slit-nozzle expansion. The observed line width of 270 MHz is due to residual Doppler broadening.

slit-jet configuration resulted in a linewidth of less than 0.01 cm^{-1} on this resonance shown in Fig 3, which is due to residual Doppler broadening in the planar jet-geometry. This example constitutes the first measurement of an optical transition in O_2, which is not limited by the full Doppler-broadening encountered when probing static gas samples. In this example only the lowest rotational energy level could be probed, due to the jet conditions, where a mixture with strongly cooling argon gas was used; this technique might be used in future to improve upon the electronic spectroscopy of the electronic transitions in O_2.

Xu *et al.* [14] performed quantitative CRD-studies on three atmospheric bands $b - X(v', 0)$ for $v' = 0 - 2$, with a laser of 0.09 cm^{-1} bandwidth, just somewhat broader than the molecular absorption feature. In the analysis of the decay transients the signal was assumed to originate from two contributions, giving rise to a bi-exponential transient: one part was assumed to be exactly on resonance and absorbing proportional to the strength of the spectral line, while the remaining part was assumed to be off-resonant. Within this model-assumption pressure dependent rotational line strengths were analyzed as a function of pressure for a number of lines in the three bands. Resulting values for the line strengths confirm the quoted values in the HITRAN database. Pressure broadening, involving self-broadening effects as well as collisions with N_2, was investigated by CRD on the $b-X(1, 0)$ band at 688 nm [15]; there is a vast literature on this subject coming from FT-studies.

2.2.2 The $a^1\Delta_g$ - $X^3\Sigma_g^-$ Infrared Atmospheric System

The $a^1\Delta_g$ - $X^3\Sigma_g^-$ (0,0) band at 1.27 μm was investigated independently by two groups using the generic pulsed cavity-ring down method [16, 17]. This near-infrared atmospheric system is, with an upper state lifetime exceeding 1 hour, even weaker than the $b-X$ system. In the study of Newman *et al.* [16] CRD was compared with long path Fourier-transform spectroscopic investigations involving 60 atm m effective path lengths. As for the sensitivity the CRD and FT methods are found to be equally suited as spectroscopic tools. In this region of the near-infrared, where the combined Doppler and collision broadened width (for atmospheric pressure) on oxygen lines is typically 0.1 cm^{-1}, most commercially available pulsed laser systems have bandwidths beyond this value. As in the case of Newman *et al.* the bandwidth of 0.25 cm^{-1} gives rise to problems in deducing quantitative information on the line intensities. This bandwidth problem has been recognized and treated formally by various groups [18, 19, 20] and is in a sense similar to the slit width problem in classical spectroscopic investigations. In CRD it entails problems related to the fact that the obtained transients are no longer mono-exponential if the bandwidth of the laser exceeds the widths of the molecular resonance. Note that Xu *et al.* [14] assessed this problem slightly differently with the assumption of a two-component decay, as discussed above.

Newman *et al.* followed the estimates and the analysis of Zalicki and Zare [19], who showed that the deviation is reasonably small and quantifiable if the absorbance per cavity round trip remains small. In such case the *integrated* intensity, i.e. across a spectral line, deviates only by an amount of less than 10%. However, to ensure the smallness of the single round-trip absorption only a portion of 0.5 μs from the entire decay transient could be used. We note that in the experiment the cavity decay time was 7 μs (mirror reflectivity R=99.93 % and 1.5 m cavity length) and hence the majority of data points, usually giving rise to improved signal-to-noise, were omitted. As a final result the total integrated band intensity on the $a^1\Delta_g$ - $X^3\Sigma_g^-$ (0,0) band could be brought into agreement with the Fourier-transform spectroscopic measurements to within 2%, yielding a value for the Einstein coefficient of $A = 2.19(7) \times 10^{-4} s^{-1}$ [16].

In the study of Miller *et al.* [17] a more state-of-the-art laser system could be applied with a nearly Fourier-transform limited bandwidth of 0.017 cm^{-1} at 1.27 μm, therewith avoiding the aforementioned bandwidth problems in the quantitative analysis of the CRD-transients. However, as was demonstrated previously by Martin *et al.* [21], when the coherence time exceeds the round trip time in the cavity, disturbing oscillations on the ring-down transients will occur, that prohibit a straightforward interpretation of the decay transient in terms of an absorbance. Miller *et al.* overcame this problem by lowering the detector response to 600 ns, therewith washing out the oscillations. It is noted that such procedure will decrease the obtainable sensitivity in the experiment, but here the focus was on a determination of the band integrated intensity and the Einstein A-coefficient. Measurements were performed over a range of pressures, varying from 15 to 557 torr, resulting in a value of $A = 2.3(3) \times 10^{-4} s^{-1}$, which is in good agreement with the average from a number of classical experiments, and confirming the study of Newman *et al.* [16].

2.2.3 The Herzberg bands in the Ultraviolet

The extension of ring-down techniques to the wavelength domain of the ultraviolet is relatively straightforward, and again the oxygen molecule provides a benchmark test system for CRD studies. Frequency doubling techniques, converting the output of commercially available tunable lasers into the ultraviolet, usually reduce the laser output by an order of magnitude, but since only milliJoules of laser intensity is required in a generic CRD-experiment, this has no adverse effect. A major point of concern is the reduced reflectivity of avaliable mirrors to a maximum of typically 99.8%; this severely limits the sensitivity of CRD in the UV. Huestis *et al.* [22] reinvestigated the spectra of the Herzberg bands close to the dissociation threshold by CRD and by an alternative technique of probing the oxygen atoms, produced by collisional dissociation involving an excited oxygen molecule. In an initial study a laser with a bandwidth of 0.5 cm^{-1} was applied, and it was demonstrated that CRD had a superior sensitivity and new features were observed. Also the first direct information on oscillator strengths of the Herzberg II and III systems was generated in these experiments. In a subsequent study [23] focusing on the 242-244 nm region, where new features had been identified, a laser of improved bandwidth (0.2 cm^{-1}) was used for the purpose of better resolving the features and for addressing the bandwidth issue in quantitative CRD. It should be noted that this narrower bandwidth is still a factor of three above the Doppler width on the molecular oxygen resonances.

In this region of the ultraviolet again a comparison can be made between the CRD-technique and the concomitant developments in Fourier-transform spectroscopy. A UV Fourier-transform spectrometer was developed [24, 25] that could be set to an effective resolution of 0.06 cm^{-1} yielding an accuracy of 0.005 cm^{-1} in the line positions. In terms of resolution this FT-setup is indeed superior to the CRD-setup used in Refs. [22, 23] although it should be noted that there do exist UV-lasers that would match this resolution. In terms of sensitivity the CRD-experiment, here limited by the mirror reflectivity of 99.6%, made possible the observation of 5 new excited vibrational levels $A^3\Sigma_u^+, v = 12$, $A'^3\Delta_u, v = 12, 13$ and $c^1\Sigma_u^-, v = 17, 18$; moreover of the $A - X(11, 0)$ band 12 branches were observed via CRD, and only 8 with FT-spectroscopy. Apart from the newly identified features the CRD-experiment yielded also some 100 additional yet unidentified spectral lines probing the range just below the dissociation threshold in O_2. As for the oscillator strengths an attempt was made in the CRD-studies to correct for the effect of the laser bandwidth, but a comparison with the higher resolution FT-study [25] indicates that there is still an underestimate of 30% on the line strengths.

The developments in CRD and FT-techniques have progressed simultaneously. After the work of Slanger *et al.* [23] Jenouvrier *et al.* [26] performed FT-studies in the UV, again focusing on the energy region below the first dissociation threshold in O_2. With an improved sensitivity some lines reported in the CRD-experiments were not observed in FT and vice versa. Nevertheless, based on the resolution of 0.12 cm^{-1} many hitherto unidentified lines could be given an assignment. From a deperturbation analysis some transitions could be assigned to a weakly bound state of $^3\Pi_u$ symmetry of which vibrational levels $v = 0$ and

$v = 1$ were identified and for which a dissociation energy of $D_e = 140\,\mathrm{cm}^{-1}$ was determined.

2.2.4 The $(O_2)_2$ Complex

Since the end of the 19^{th} century it was known that high-density oxygen gas features some additional absorption phenomena. Broad resonances, investigated in the condensed phase and in the high-pressure regime, are understood as due to O_2-O_2 collisional complexes. During a collision an electronic transition is induced in the $(O_2)_2$ system. This is an effect of symmetry breaking by the collision partner, giving rise to a change of the selection rules. As a result both O_2 partners may leave in an electronically excited state after absorption of a single photon. At the 630 nm resonance both molecules are excited to the $a^1\Delta_g, v = 0$ state. Naus and Ubachs [27] employed the sensitivity of pulsed CRD to investigate the $(O_2)_2$ features at 630 and 580 nm in the pressure regime below 1 atm. Density-dependent cross-sections were determined at discrete wavelength settings from an analysis of measured CRD-extinction curves as a function of pressure as shown in Fig. 4. The derived cavity-decay times have a quadratic dependence on gas pressure due to the

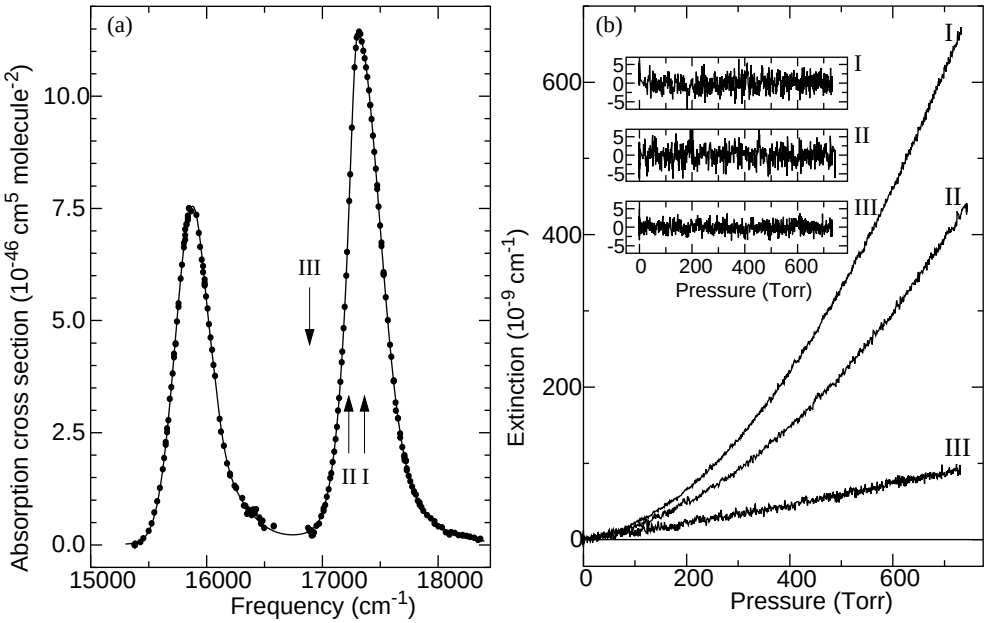

Figure 4: Observation of two prominent $(O_2)_2$ collisional induced features with Cavity-Ring Down spectroscopy; (a) density dependent absorption cross sections as a function of wavelength (dots) and a fit to skewed Voigt profiles (full line); (b) Extinction measured as a function of pressure at three frequency positions (I, II and III) also shown in spectrum (a); while at position III extinction is nearly linear (only Rayleigh scattering) at position I the quadratic behavior is evident; in the inset the residuals from a least-squares fit. Reproduced with permission from Ref. [27].

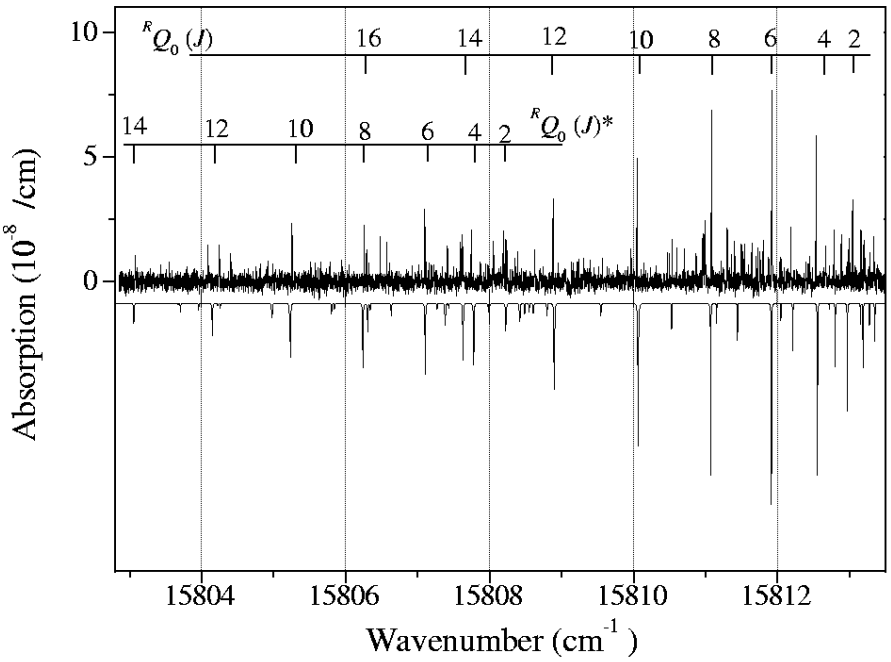

Figure 5: Part of the CW-CRDS spectrum of the $(O_2)_2$ Van-der-Waals complex. The assigned lines pertain to two different sub-bands of the $[a^1\Delta_g, v=0]_2 \leftarrow [X^3\Sigma_g^-, v=0]_2$ transition. In the lower panel a calculated/fitted spectrum is shown. Reproduced with permission from Ref. [29].

collisional phenomenon involving two molecules; however the extinction is so weak that a linear contribution, related to Rayleigh scattering had to be included in the analysis; also a constant term related to the mirror reflectivity was included in the fits to the data.

The CRD-method appears to be ideally suited for such measurements: (i) for the broad resonances there is no bandwidth problem and the extinction can be straightforwardly interpreted in terms of cross sections; (ii) the contributions of Rayleigh scattering and collision-induced absorption can be unraveled; (iii) by choosing discrete frequency positions of the laser the features of the $(O_2)_2$-complex at around 630 nm can be disentangled from the linearly absorbing γ-band in the O_2-monomer, also at 630 nm. The latter entails a marked advantage over the FT-technique, which was also applied to investigate $(O_2)_2$ [28].

While the $(O_2)_2$ collisional complex is associated with the repulsive part of the O_2-O_2 intermolecular potential Van-der-Waals bound states do exist below the dissociation threshold within this potential. Sharp and well-resolved absorption spectra of the O_2-dimer have been recorded in a supersonic slit jet expansion using the continuous wave (CW)-CRD technique [29]. Here the slit-jet configuration provides sub-Doppler resolution on the resonances of below 0.01 cm^{-1} as shown in Fig. 5. From a rotational analysis of

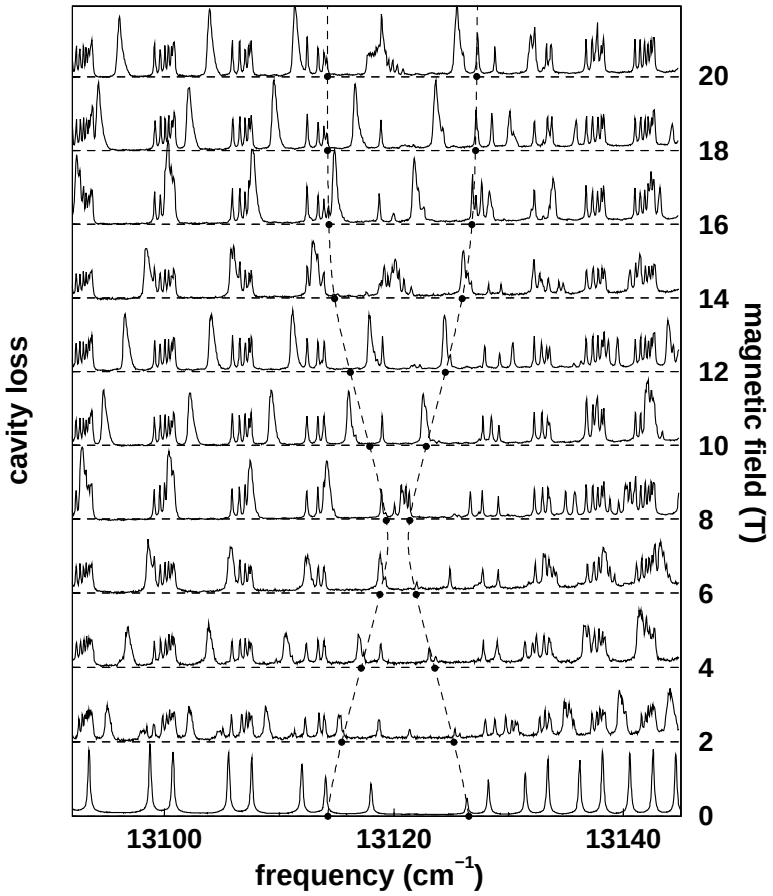

Figure 6: Right-hand circularly polarized light has been used to measure the CRD spectrum of the central part of the $b^1\Sigma_g^+(v{=}0) \leftarrow X^3\Sigma_g^-(v{=}0)$ transition of molecular oxygen as function of the magnetic field. Two transitions with the same upper state are indicated by the dashed lines. Figure reproduced from Ref. [30] with permission.

these spectra, the geometrical structure could be determined in the ground and excited states. For the $[X^3\Sigma_g^-, v = 0]_2$ ground state configuration a geometry in the form of an H, with an inter-monomer separation of 6.04-6.14 a_0 was determined as the most stable one. In this study [29] also a comparison was made between the intracavity laser absorption technique and CW-CRDS. Although sensitivities were similar the grating spectrograph in ICLAS limits the resolution, rather than the laser as in CW-CRDS; hence the resolution in CW-CRDS was better by more than a factor of two.

2.2.5 O_2 in Magnetic Fields

Even though the light in most of the CRD experiments is polarized, there are not many spectroscopic studies which make use of this property. Berden *et al.* [30] have recorded the

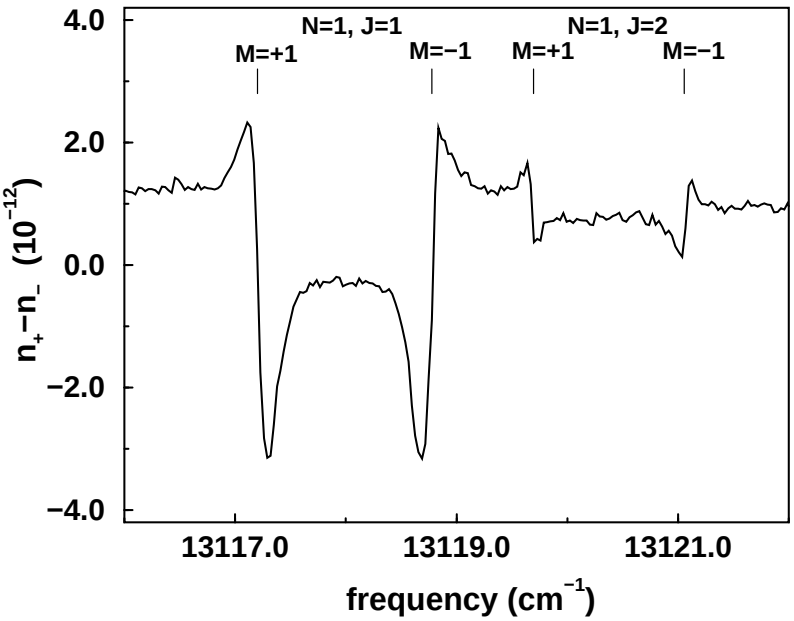

Figure 7: PD-CRD dispersion spectrum in the region of the ${}^{P}P(1,1)$ transition in the A band of molecular oxygen at 200 mbar. Measurements are performed in a 3 cm cavity which is placed in a magnetic field of 1.5 T. The magnetic field, which is parallel to the cavity axis, splits the transition into two components. The two small dispersion curves belong to the ${}^{P}O(1,2)$ transition, which becomes allowed through magnetic field induced mixing with the ${}^{P}P(1,1)$ transition. The dispersion curves are labeled with the quantum numbers of the $X^3\Sigma_g^-$ state. Figure reproduced from Ref. [30] with permission.

rotationally resolved CRD spectra of the A band of molecular oxygen in magnetic fields up to 20 Tesla. Spectra were measured with linearly and circularly polarized light, leading to different ΔM selection rules, thereby aiding in the assignment of the spectra. The Bitter-type magnet has a 80 cm long bore with a diameter of 3.1 cm. Since the magnetic field was homogeneous only over a few centimeters at the center of the bore, a very short cavity has been used in order to prevent the spectra from becoming too complex. Therefore, the mirrors were mounted on a 3 cm long tube, in a fixed position relative to each other. This short cavity was placed at the center of the magnet. The axis of the cavity was parallel to the magnetic field lines, i.e. the so-called Faraday configuration.

Figure 6 shows the spectra recorded with right-hand circularly polarized light (σ^+) as a function of the magnetic field strength. Only the central part of the A band is displayed. Due to the specific polarization of the light, only transitions with ΔM=+1 are allowed. Although not shown here, Berden *et al.* [30] also measured the CRD spectra using left-hand polarized light and linearly polarized light, containing transitions with ΔM=–1 and ΔM=$\pm$1, respectively.

These spectra have been used to validate a theoretical model that is used to describe

the interaction between the oxygen molecule and the magnetic field, by comparing the calculated and measured line positions and intensities. This model has further been used to calculate the spin contribution to the magnetic susceptibility of molecular oxygen. It also shows that the oxygen molecules are aligned in high magnetic fields, and that this alignment is caused by the spin-spin interaction via a coupling of the spin angular momentum to the magnetic field direction [30].

By placing a polarization selective optical element in front of the detector (e.g. a polarizer), it is possible to measure the rotation of the plane of polarization of the incoming linearly polarized beam upon passage through the ring down cavity. If (part of) the cavity is placed inside a magnetic field, the plane of polarization can rotate owing to dispersion (magnetic birefringence) or polarization dependent absorption (magnetic dichroism). This has been exploited by Engeln *et al.* [31], who have placed the cavity between two polarizers. The light exiting the cavity was split into two mutually orthogonal polarized components, and the time dependence of these components was measured simultaneously.

In this so-called Polarization Dependent cavity ring down (PD-CRD) scheme, the information is obtained from the difference between the cavity losses in the two directions. It has been theoretically shown and experimentally demonstrated [31] that this difference is proportional to the magnetic dichroism in the case that the magnetic field lines are perpendicular to the cavity axis (Voigt configuration), and it is proportional to the magnetic birefringence in the case that the magnetic field lines are parallel to the cavity axis (Faraday configuration). An example is shown in Figure 7, where part of the PD-CRD dispersion spectrum (magnetic birefringence) of molecular oxygen is shown [30]. This spectrum is recorded at 1.5 T by using the aforementioned 3-cm long cavity in a Bitter magnet. It is evident that PD-CRD is only suitable to record spectra of paramagnetic molecules. Absorptions of other species are detected in both polarization directions and cancel out in the difference spectrum. In principle, PD-CRD spectroscopy is the CRD variant of magnetic rotation spectroscopy (MRS). Just like MRS, PD-CRD can be used to simplify spectra because both techniques are more sensitive for transitions with low rotational quantum numbers, and to distinguish spectral features of paramagnetic species from those of non-paramagnetic species.

2.2.6 Spectroscopy of Oxygen with CW Lasers

In CW-CRD spectroscopy, the cavity is excited with a CW laser. Just as in pulsed CRD spectroscopy, the ring down time, and thus the absorption coefficient of the molecules present in the cavity, is determined by measuring the decay of the light exiting the cavity (see e.g. ref. [32]). However, CRD spectroscopy with CW lasers can as well be performed without temporal analysis of the ring down transient. In phase shift cavity ring down spectroscopy (PS-CRD), the absorption coefficient is extracted from a measurement of the wavelength dependent phase shift that an intensity modulated CW light beam experiences upon passing through a high finesse optical cavity. The phase shift method has been used to record the absorption spectra of the δ band of $^{18}O_2$ [12].

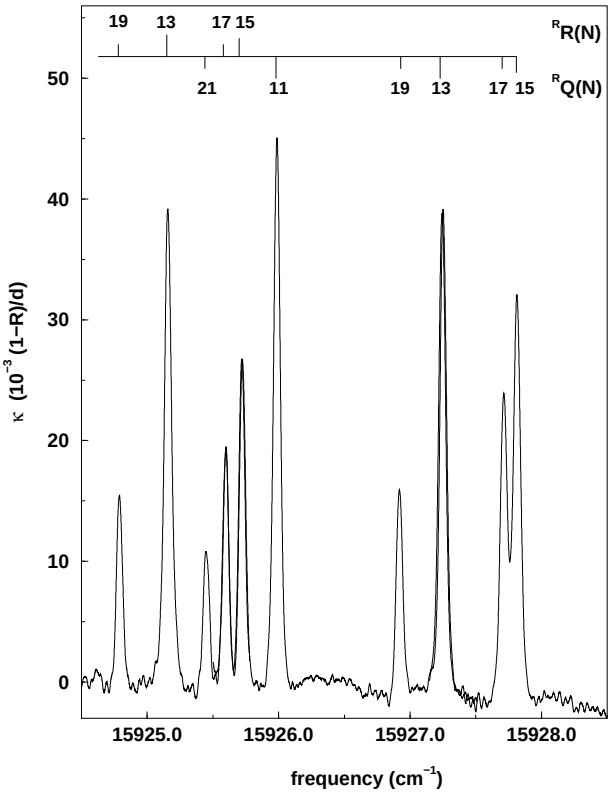

Figure 8: CEA spectrum of the oxygen γ-band recorded in a cell of 12 cm length with 200 mbar pure oxygen, displaying the bandheads in the ${}^{R}R$ and ${}^{R}Q$ branches near 628 nm. Figure reproduced from Ref. [13] with permission.

In CW-CRD spectroscopy an optical switch is required to prevent the in-coupling of light into the cavity while the decay transient is recorded. In PS-CRD spectroscopy an intensity modulator is required. In Cavity Enhanced Absorption (CEA) spectroscopy no such device is needed. In the latter spectroscopic method the absorption coefficient is determined from a measurement of the *time-integrated* intensity of the light leaking out of the cavity, while light is coupled into the cavity via accidental coincidences of the laser frequency with the frequency of one of the multitude of modes of the cavity [13]. It has been shown that this time-integrated intensity is proportional to the cavity ring down time τ and thus inversely proportional to the total cavity losses [13, 33]. Note that the name CEA spectroscopy is also frequently used to label all techniques using a cavity to enhance the absorption (like the title of this book), while in this chapter CEA is only used to describe the aforementioned technique (see also Ref. [34]).

Figure 8 shows the bandheads of the ${}^{R}R$ and ${}^{R}Q$ branches of the γ band of $^{16}O_2$ recorded with the CEA technique. The spectrum consists of three partly overlapping measurements, each covering about 1.5 cm^{-1}, and have been recorded with a CW single mode ring dye laser

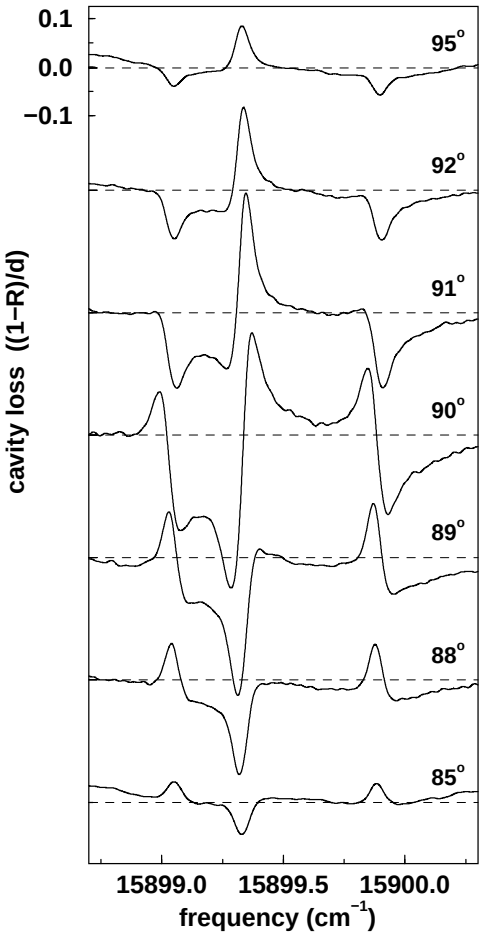

Figure 9: CEMR spectra of the $^{P}P_1(1)$ transition of the γ band of O_2 recorded in a magnetic field of 0.88 T (Voigt configuration), as function of the angle ϕ_D (With crossed polarizers ϕ_D=90°). Figure reproduced from Ref. [13] with permission.

in about 1 minute. The absorption coefficient is expressed in units of $(1–R)/d$, with R the mirror reflectivity and d the distance between the mirrors. Therefore CEA spectroscopy is not a self-calibrating technique in contrast to the generic form of CRD spectroscopy; the mirror reflectivity has to be known in order to make the absorption axis absolute (the mirror reflectivity can be determined in a CRD experiment, or in a CEA experiment with a known molecular absorption; see Ref. [13]).

The CEA method can also be combined with MRS which results in cavity enhanced magnetic rotation (CEMR) spectroscopy [13]. As an example, we will discuss a CEMR spectrum of the $^{P}P_1(1)$ transition of the γ band of $^{16}O_2$. The cavity is placed inside a homogeneous magnetic field of 0.88 T in such a way that the magnetic field lines are perpendicular to the cavity axis (Voigt configuration). The polarization of the CW light

that enters the cavity makes an angle of 45° with respect to the magnetic field. Therefore, transitions with ΔM=0,±1 are allowed. A polarizer between the exit of the cavity and the detector transmits the light with a polarization direction of ϕ_D relative to the polarization direction of the incoming light.

In Figure 9 the inverse of the time-integrated light intensity passing through the analyzer is shown as function of frequency in the spectral region of the $^PP_1(1)$ transition for seven different values of the angle ϕ_D [13]. For a value of ϕ_D sufficiently far away from 90°, the inverse of the time-integrated signal is proportional to the polarization dependent absorption (magnetic dichroism). The spectrum measured with crossed-polarizer geometry, exclusively shows the effect of optical rotation due to dispersion [13]. Note that the spectrum with ϕ_D=90° measured with the Voigt configuration can directly be compared with the dispersion spectrum shown in Figure 7 which has been measured for the same transition (but then for the A band) with the Faraday configuration.

2.2.7 Toward Ultimate Sensitivity and Accuracy

In the above the application of the generic pulsed cavity ring-down technique and some variants using CW-laser sources were described in the measurement of weak absorption in O_2. Along with detection of the multiply forbidden quadrupole bands at 760 nm in a pulsed CRD-experiment, with mirrors of R = 99.998%, a test of the detection limit on the even rotational lines in O_2 was performed [5]. These lines are strictly forbidden by the symmetrization postulate of quantum mechanics and they serve as a test for this fundamental principle. In the experiment of Ref. [5] a sensitivity of 1.5×10^{-6} was obtained.

It was already mentioned that in the pre-CRD era some important developments in intracavity dye laser spectroscopy were pursued in which nearly comparable absorption sensitivity was achieved on the forbidden O_2 bands in the visible [3, 4]. Following up on these CRD-precursor techniques sophisticated cavity-enhanced techniques have been developed, using locking of the cavity to a CW-laser, phase modulation and heterodyne signal detection, in which the absorption sensitivity was increased to 7×10^{-11} cm^{-1}Hz$^{-1/2}$; using this setup a test on the even lines in O_2 was performed at the 5×10^{-8} level [35]. Further progress in this area of highly sensitive cavity-enhanced techniques are discussed elsewhere in this book.

Van Zee *et al.* [36] have assessed the issue of quantitative precision in a CRD-experiment and have argued that a single-mode approach yields the highest precision. For most spectroscopic purposes, where the focus is on easy tunability of the spectrometer, the CRD-cavity is set such that it can be excited by a large number of modes giving the cavity a white spectrum; the whiteness of a high-finesse cavity, set far from confocal, was experimentally demonstrated [37]. The more cumbersome single-mode approach, where the cavity length has to be kept at the same mode of the resonator and in lock with the laser mode, is however shown to produce a quantitative reproducibility with a 3×10^{-4} standard deviation in the ring-down time in a measurement of the $^PQ(9)$ line in the oxygen A band. The authors have discussed on the possibility of using such a CRD-setup as a pressure standard.

2.3 Spectroscopic Applications of CRD

The CRD technique is especially powerful in gas phase spectroscopy for measurements of either strong absorptions of species present in trace amounts or weak absorptions of abundant species. For spectroscopic applications of the CRD technique this roughly means that species with relatively weak transitions are studied in static gas cells (for example molecular oxygen), since one can simply increase the number density of the species. On the other hand, species with strong transitions are studied in supersonic jets, discharges, or flames, since the number densities in these environments are usually relatively low. In the remaining part of this chapter, an overview will be given of pure spectroscopic applications of CRD spectroscopy in, respectively, static gas cells, flames and discharges, and in supersonic jet expansions.

2.3.1 In Static Gas Cells

In 1988 O'Keefe en Deacon reported the first CRD spectra [2]. They measured the spectra of the B and γ band of molecular oxygen in a static gas cell. As exemplified in the previous section, molecular oxygen has always been one of the favorite molecules for CRD spectroscopy, but many other molecules have been investigated as well. Besides the determination of spectroscopic constants from the frequency position of the observed transitions, an important feature of static cell experiments is the determination of absolute line and band intensities (which is made possible due to the accurately known number density).

In a series of publications, Romanini and Lehmann reported the absorption spectra of HCN and its isotopomers in the 435-571 nm spectral region [38, 39, 40, 41]. This spectral region contains many very weak overtone bands. Figure 10 shows the CRD spectrum of the 106←000 transition of HCN (1 quantum in the CN stretch, 0 in the bending mode, and 6 quanta in the CH stretch). By recording this spectrum at different pressures, it was shown that there is a large collisional line-mixing effect in the proximity of the R branch heads.

Campargue *et al.* [42] recorded the $5\nu_1$ band of propyne by using the pulsed CRD technique. The same method was used by Kleine *et al.* [43] to measure the absolute intensity of the fifth CH stretching overtone of benzene and by Naus *et al.* [44], who reinvestigated the weak overtone spectrum of water vapor in the wavelength range 555-604 nm. Brown *et al.* [45] determined the absorption cross sections for the third and fourth O–H overtone transitions on nitric acid and hydrogen peroxide, while the O–H stretching vibrational overtones of 2-butanol were studied by Xu *et al.* [46]. With a tunable CW diode laser He *et al.* [47] recorded the spectra of the $\nu_1+3\nu_3$ band of N_2O and $CHCl_3$ around 1.3 μm.

2.3.2 In Hostile Environments

Triggered by the success of the detection of radicals in laser ablation sources [48], laser photolysis reactors [49] and flames [37], CRD spectroscopy has become a powerful tool

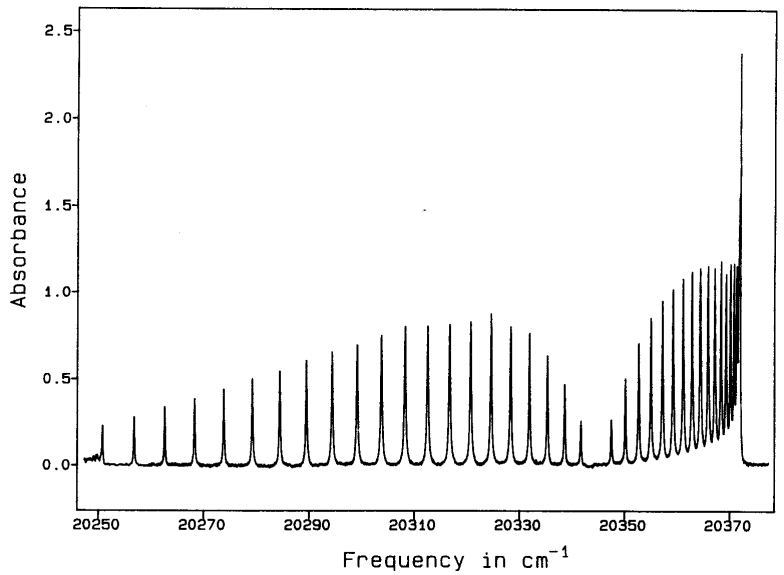

Figure 10: The CRD absorption spectrum of the 106←000 transition of HCN. The sample pressure was 100 Torr. Figure reproduced from Romanini and Lehmann [38] with permission.

to perform spectroscopic measurements in hostile environments. Zalicki *et al.* [50] first investigated CRD absorption of methyl radicals (CH_3) in a flow reactor, where CH_4/H_2 mixtures flow over a hot tungsten filament at 2300 K. The broad absorption feature at 216 nm was used for a quantitative analysis of CH_3-densities. Similarly the silyl radical (SiH_3) was probed, via its broad resonance at 215 nm, in a remote Ar-H_2-SiH_4 plasma during hydrogenated amorphous silicon thin film growth [51]. Booth *et al.* [52] probed various fluor-containing radicals (CF, CF_2, AlF and SiF_2) in radio-frequency plasmas in fluoro-carbon gases; these molecules have strong absorption features in the 215-230 nm region as well. The application of ring-down techniques for the spectroscopy of species in harsh environments requires some special precautions to protect the highly reflecting mirrors. Deposition of contaminants, that cause a reduction of their reflectivity, can be circumvented by the use of diaphragms inside the vacuum chamber and helium curtains near the mirrors [45, 53, 54].

The study of predissociation in excited states of molecules using CRD has become a topic in itself. Spaanjaars *et al.* [55] have determined the predissociation rates of OH ($A^2\Sigma^+, \nu'=3$) for N' up to 17 by simultaneously measuring laser induced fluorescence (LIF) and CRD absorption in the same laminar CH_4/air flame. The relative intensities in the LIF and CRD spectra are different, which is due to the rotational dependence on the predissociation rate; with varying rotational quantum number, the competition between predissociative and radiative decays has a strong effect on the intensity of the fluorescence signal. CRD measures direct absorption and the signal intensity is independent on the

relaxation of the excited state. Hence the combination of the two techniques, CRD and LIF, provides a sensitive tool for predissociation phenomena.

Extensive predissociation studies of a large number of molecules have been reported by Orr-Ewing and co-workers (reviewed by Wheeler *et al.* [56]). A nice example is the molecule HNO. In Figure 11, a LIF spectrum and a CRD spectrum measured in the same spectral region are shown. Much of the structure present in the CRD spectrum is absent in the LIF spectrum because of predissociation of the $\tilde{A}'$ state [57]. Besides missing lines in the LIF spectrum, predissociation can also be observed via an increased line width of the rotational transitions (due to the short life time of the predissociating upper state). A detailed study of predissociation offers a valuable approach to explore state-selected unimolecular chemical reaction dynamics on coupled potential energy surfaces [56]. The group of Orr-Ewing has studied many other molecules, which were generated in a flow reactor, like SH and SD [58, 59], S_2 [60], BrO [61], IO [62], ClO [63], HClCO [64], and FCO [65].

Kotterer and Maier [54] have detected the $^2\Pi - X^2\Pi$ electronic transition of the carbon chain C_6H by pulsed CRD spectroscopy at 526 nm. This radical, which is of astrophysical interest, was generated in a hollow cathode discharge of acetylene in helium. They used the same experimental setup to study weak vibrational bands of the electronic $A^2\Pi_u \leftarrow X^2\Sigma_g^+$

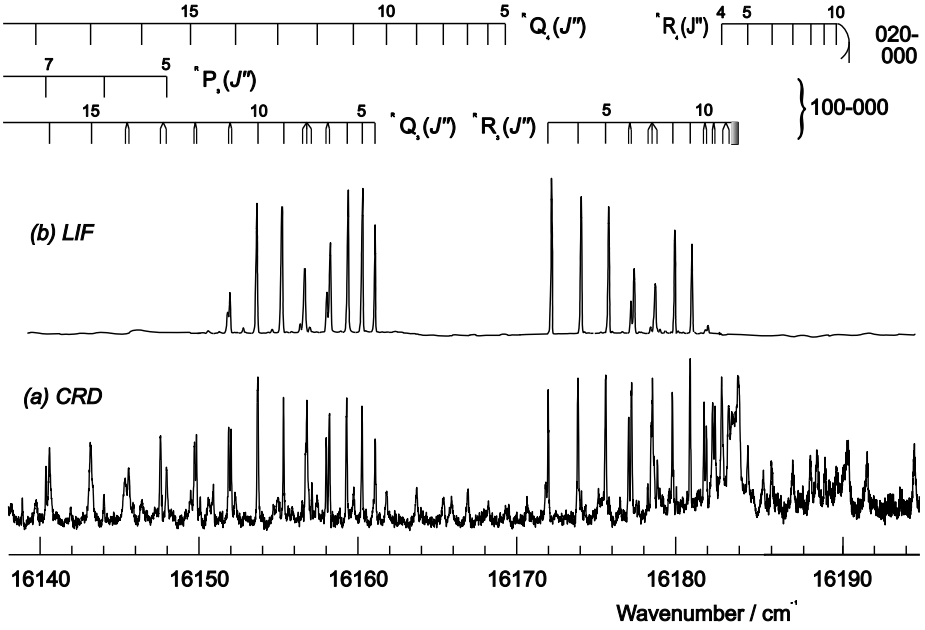

Figure 11: LIF (top) and CRD (bottom) spectra of the HNO molecule with transitions form the $\tilde{X}'\ ^1A'$ (000) ground state to vibrational levels (100) and (020) of the $\tilde{A}\ ^1A''$ excited state. Because of predissociation part of the structure is absent in the LIF spectrum. Reproduced with permission from Ref. [57].

transition of the molecular ion N_2^+ [66]. Additional bands were measured in a similar setup by Aldener *et al.* [67]. CRD spectroscopy has also been used to determine the dipole transition moment of photochemically produced sodium hydride [68]. In this experiment, NaH was formed by laser excitation of sodium, generated in a heat-pipe oven, in a hydrogen atmosphere. Strong saturation effects (power broadening and dips at the center frequency) were observed [69]. Similar saturation effects have been observed for Li_2 which was also produced in a heat-pipe oven [70].

2.3.3 In Jet Expansions

Supersonic molecular beams and jets are very important in molecular spectroscopy. Expanding molecules seeded in a carrier gas (mostly a noble gas) into vacuum produces a cooling of the vibrational and rotational degrees of freedom. The advantage for spectroscopy is two-fold. On the one hand, only the lowest rotational and vibrational levels in the electronic ground state are populated, leading to less congested excitation spectra. On the other hand, the low internal temperatures permit the stabilization of structural variants (tautomers or conformers) and the stabilization of molecular clusters (van der Waals and hydrogen bonded clusters).

Already in 1990, Saykally and co-workers reported their first results on the electronic spectroscopy of jet-cooled metal clusters which were produced by laser vaporization of a metal rod [48]. Since then, many metal clusters were investigated such as PtSi [71], AuSi [72], AgSi [73], CuSi [74], Al_2 [75], WO [76], and Cr_2 [77]. This metal cluster research has been reviewed by Scherer *et al.* [78, 79].

While this work was performed in the visible region of the spectrum, their more recent work is focused on the infrared region, where vibrational transitions can be probed. Pulsed tunable infrared light (2-7 μm) is efficiently generated by Raman shifting of the pulsed dye laser output. The extension of the CRD-technique towards the near and mid-infrared has been used to measure the O-H stretching vibrations in clusters of water [80] (see Fig. 12), methanol [81], ethanol, and butanol [82]. Other studies are, for example, the monomer bending vibration in water clusters [83], and the carbonyl stretch in arginine [84].

Aromatic molecules have been studied with CRD spectroscopy as well. Although a REMPI scheme was much more sensitive to record the vibrationally resolved spectrum of the $S_1 \leftarrow S_0$ of diphenylamine (DPA), Boogaarts and Meijer additionally used CRD spectroscopy to determine the absolute number density of DPA molecules in their laser desorption jet-cooling molecular beam spectrometer [85]. Ruth *et al.* [86] recorded CRD spectrum of the $T_1 \leftarrow S_0$ transition of jet-cooled 4-H-1-benzopyrane-4-thione, which was compared with the REMPI spectrum and the phosphorescence excitation spectrum. They also used the CRD technique to study the internal conversion rate as a function of excess energy for the azulene molecule [87]. In the 545-680 nm spectral region, Romanini *et al.* [88] recorded the absorption spectrum of naphthalene cations, which were produced in a slit jet coupled to an electronic discharge.

The spectroscopy of azulene molecules and naphthalene cations is also interesting from

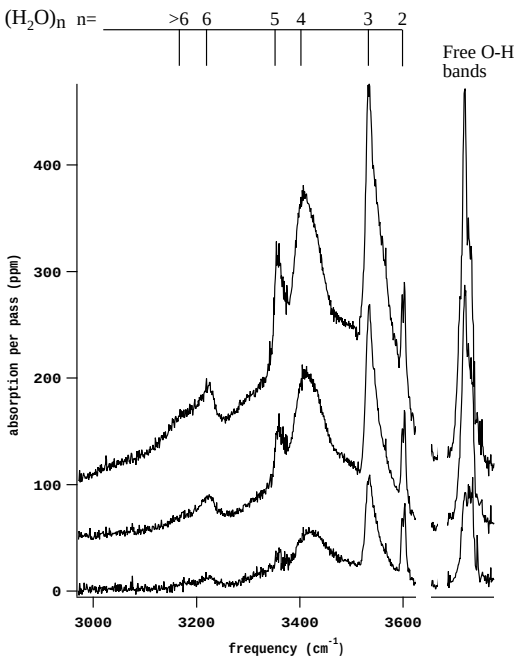

Figure 12: CRD spectra of the O-H stretch in water clusters obtained for various source backing pressures; n indicates the number of H_2O molecules in a cluster. Figure reproduced from Ref. [80] with permission.

an astrophysical point of view; the absorption spectra can directly be compared with the diffuse interstellar bands (DIB), the ubiquitous absorption features in the spectra of many stars, whose origin is still a mystery. A couple of hundred DIBs have been observed, primarily in the 400-900 nm region. Besides aromatic molecules, carbon chains are promising candidates as well. Linnartz and Maier and co-workers have investigated species which were generated by a discharge in a supersonic expansion of gas mixtures through a slit nozzle. With the CRD technique they measured the (rotationally resolved) electronic spectra of C_6H and C_6D [89] (see also Figure 13), C_8H and $C_{10}H$ [90], $C_6H_2^+$ and C_2^- [53], $C_8H_2^+$ [91], C_4 [92], C_5 [93], HC_6N and HC_7H [94] and various carbon containing chain molecules [95]. A similar setup has been used by Ball *et al.* to record electronic spectra of HC_nH (n=7,9,11,13) [96, 97].

Other CRD spectroscopic studies report on the T_1 state of thiophosgene (Cl_2CS) [98], the S_1 state of acrolein (CH_2CHCHO) [99], the $\tilde{C}\ ^1A'$ state of S_2O [100], the first overtone of the free hydrogen stretch of several $(HCl)_2$ isotopomers [101], and the infrared spectrum of the formic acid dimer [102]. By using CW-CRD spectroscopy, Romanini *et al.* [103] investigated saturation effects in jet cooled NO_2, and Hippler and Quack [104] studied the $\nu_2+2\nu_3$ combination band of methane around 7510 cm^{-1}.

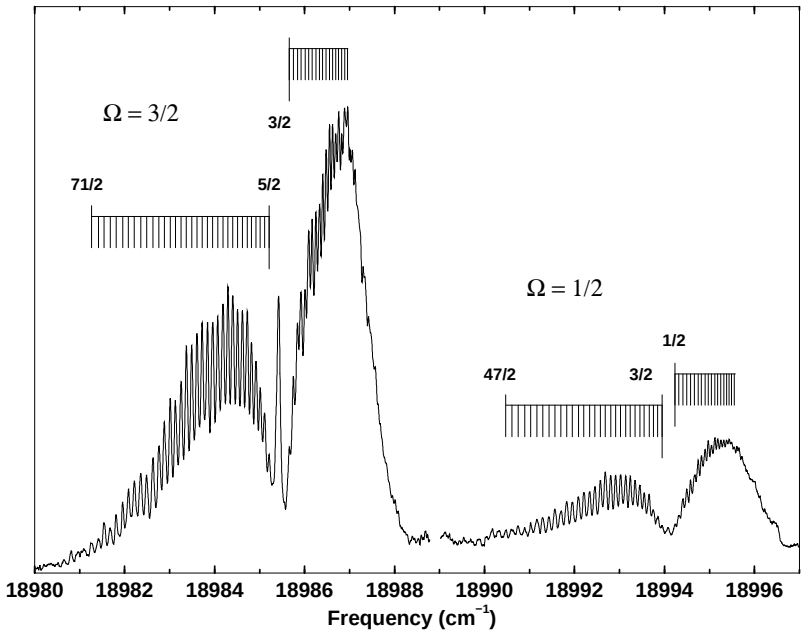

Figure 13: The two spin-orbit components in the $^2\Pi \leftarrow X^2\Pi$ transition of C_6H measured with CRD spectroscopy in a supersonic slit jet plasma. Reproduced with permission from Ref. [89].

2.3.4 Quantitative Study of Rayleigh Scattering

Rayleigh scattering is usually considered a nuisance in CRD experiments. It gives rise to a non-resonant background and is in a sense similar to the contribution of mirror reflectivity to the decay transient. Ultimately it is a factor limiting the sensitivity of CRD-experiments. The Rayleigh-scattering cross section is closely connected to the index of refraction, scales with ν^4 (ν being the frequency) and at the few % level a correction factor is invoked for Rayleigh scattering off non-spherical particles. While the value of the Rayleigh cross section can be derived from these parameters, well-known for most molecules, a direct measurement of the Rayleigh extinction was not performed until the sensitive technique of CRD was applied [105]. For the gases Ar, N_2 and SF_6, that undergo no absorption in the visible wavelength range, the extinction was measured in a CRD-cavity as a function of pressure; results are shown in Fig. 14.

The slope of the cavity decay rate is proportional to the product $c\sigma_\nu N$, where c is the speed of light, N the number density and σ_ν the frequency-dependent Rayleigh cross section; the intercept from a fit to the decay rate, shown in Fig. 14(a), again represents the mirror reflectivity, which can be subtracted in the analysis. For various frequencies the pressure dependent extinction yields values for σ_ν, which can subsequently be invoked in a general expression for the frequency-dependent Rayleigh cross section, scaling as $\bar{\sigma}\nu^{4+\epsilon}$. Here ϵ represents the frequency dependence of the index of refraction, giving rise to a deviation from a proper ν^4-dependence.

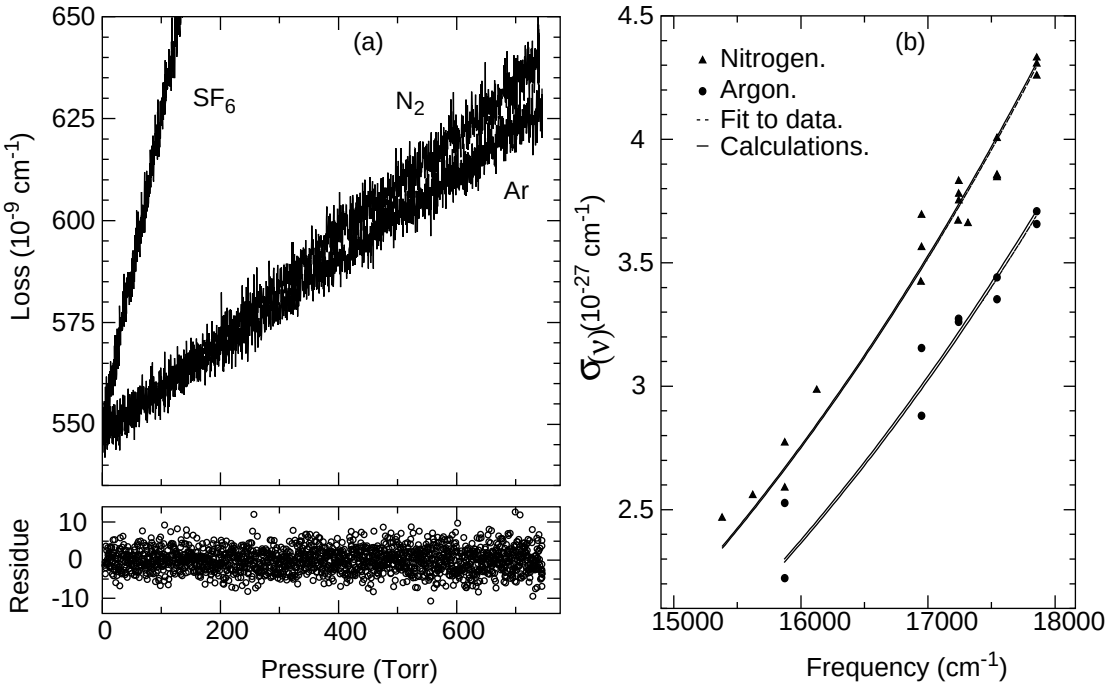

Figure 14: Measurement of the Rayleigh scattering cross section; (a) CRD-loss rate as a function of pressure for SF_6, N_2 and Ar at $\lambda = 579.83$ nm; in the bottom part are shown the residuals of an unweighted linear regression for the Ar-data with a resulting rms error of 3×10^{-9} cm^{-1}; (b) Resulting cross sections as determined from CRD-measurements at various wavelengths, and a comparison with cross sections calculated from known refractive indices. Reproduced with permission from Ref. [105].

In Fig. 14(b) the resulting values for $\bar{\sigma}$, obtained from a fit to the derived values for σ_ν are compared with calculations from known indices of refraction. This CRD-approach to Rayleigh scattering confirms these estimates, including depolarization correction factors. Moreover the experiment produces a similar level of accuracy (1%) as the calculated Rayleigh cross sections for the two gases N_2 and Ar. For SF_6 no accurate data on the refractive indices are available in this wavelength region; here such a value can be determined from CRD.

2.3.5 Spectroscopic Applications of Other Cavity Enhanced Methods

In the previous sections an overview of applications of pulsed and CW CRD spectroscopy has been given. Also the other techniques which were illustrated before by an application involving oxygen, have been used in spectroscopic studies. For example, the PS-CRD technique has been used to record the spectra of the $\Delta\nu$=6 C–H stretching overtones of C_2H_4, C_2H_6, C_3H_8, n-C_4H_{10}, and n-C_5H_{12} [106]. The CEA technique has been used by Berden *et al.* [107] to measure the absorption spectra of rotationally cold $^{14}NH_3$ in the

1.5 μm spectral region. In the slit-nozzle expansion, the linewidth of the recorded rotational lines is determined by the residual Doppler broadening and amounts to 0.006 cm^{-1}. As a result of this narrow linewidth and due to the low rotational temperature, the recorded transitions could easily be assigned. In this way, they were able to characterize the $\nu_1+\nu_3$ band at 6609 cm^{-1} and the $|l|$=2 component of the $\nu_1+2\nu_4$ band at 6557 cm^{-1}. In the same spectral region, Peeters *et al.* [108] have recorded the CEA spectra of water at room temperature and at 1100 K. The spectra are compared to simulations using data from the HITRAN and HITEMP databases, showing several discrepancies. This is, however, not too surprising since the high temperature data is primarily based on calculations. These results show that CEA spectroscopy, but also CRD spectroscopy, is a promising technique to obtain experimental data at high temperatures.

As a result of the fundamental differences between magnetically induced polarization effects and field free polarization effects, the PD-CRD approach can not be applied to the study of optical activity induced by chiral compounds. Without a magnetic field, the overall polarization rotation will cancel out during each round trip through the cavity, thereby precluding the study of field free optical activity. In order to measure the field free polarization rotation, the direction of the optical rotation must be reversed upon each reflection at the cavity mirror. This can be accomplished by placing a quarter-wave plate in front of each cavity mirror. The path length in which the optical rotation takes place is determined by the separation between the two intracavity quarter-wave plates. It is evident that these intracavity components must have a highly efficient anti-reflection coating.

Vacarro and co-workers [109] used this approach to measure the optical rotation and the differential absorption induced by chiral compounds in the gas phase. A calcite prism and a multiple-order quarter waveplate were used to produce laser light with a well-defined circular polarization. A quarter waveplate and a prism placed behind the exit mirror of the cavity projected the light exiting the cavity into two orthogonal components, which were detected by two photomultiplier tubes. Both the detected signals displayed rapid oscillations superimposed on the decay curves. These oscillations result from the change in polarization upon each round trip in the cavity, and their period is a measure for the amount of optical rotation. With this cavity ring-down polarimetry (CRDP) technique Vacarro and co-workers demonstrated a sensitivity of 4×10^{-8} rad cm^{-1}. They determined the specific rotation at 355 nm for α-pinene, β-pinene, *cis*-pinane, limonene, fenchone, and propylene oxide. From a comparison of their results with the results of solution-phase measurements, they concluded that solvent effects can be significant and nonintuitive.

2.4 CRD and Alternative Techniques

Cavity ring-down laser spectroscopy was invented at a time when laser-induced fluorescence (LIF), resonantly enhanced multi-photon ionization (REMPI), degenerate four-wave mixing (DFWM) and coherent anti-Stokes Raman spectroscopy (CARS) were fully established laser techniques for the detection of molecular species in the gas phase. An important aspect of CRD is that it measures the absorption cross section directly and is not dependent

on any excited state relaxation process (as in LIF and REMPI) nor of the influence of other electronic states in the molecule (CARS and REMPI); also the signal is proportional to the molecular density (as opposed to CARS and DFWM). CRDS works equally well in the infrared (as opposed to REMPI) as long as lasers, mirrors and detectors are available. As shown in this chapter CRD is sensitive and versatile (all molecules have absorption bands and the long list of examples speaks for itself), but there are certain drawbacks in some experimental conditions.

One shortcoming might be that the signal is integrated along the pathlength in the cavity and that no localized region of space can be probed such as in the focusing techniques (REMPI, DFWM, CARS). The absorption spectrum of a mixture of gases cannot be decomposed according to species such as is the case in REMPI, where mass-selection can be applied. The sensitivity is related to the length of the ring-down transients, which in many cases extends over 100 μs; in experiments, where short-lived species are to be detected, this absorbing period might be too long.

Even for the very weak transitions, the CRD-technique is yet powerful, but does not automatically outcast the Fourier-transform spectroscopic techniques in terms of sensitivity nor of accuracy, particularly if long absorption path lengths and large samples can be applied. In many cases both methods are equally powerful and the data from both methods can be used for validation of results; this issue was addressed in the section on O_2 spectroscopy.

Under some special conditions, where the experiment is limited for some reason, CRD might bring a strong advantage. Measurements on small samples, e.g. containing expensive isotopes, were mentioned. The availability of a strong homogeneous magnetic field over a limited length of 3 cm was favorably applied using cavity enhancing absorption techniques for the study of the Zeeman effect in O_2 in fields up to 20 T [30]; here FT-spectroscopy would have failed. As for resolution FT easily reaches the Doppler-limit in any wavelength region. The resolution in CRD studies depends on the bandwidth of the laser applied. For the generic pulsed CRD-studies usually the easily available tunable pulsed lasers are used with a typical bandwidth of 0.1 cm^{-1} in the visible range and larger in the UV. The development of CW-CRD techniques gives easy access to more narrow-band lasers such as diode lasers. As for sensitivity FT-techniques depend on the possibility to obtain long absorption path lengths and here the availability of highly reflecting mirrors, required for multi-pass setups, is important. In CRD the sensitivity is directly linked to the mirror reflectivity; hence both techniques rely on the advances in coating technology.

Acknowledgment

The Netherlands Foundation for Fundamental Research on Matter (FOM) and the Space Research Organization Netherlands (SRON) are gratefully acknowledged for financial support.

References

[1] Partridge, H., Bauschlicher, C.W., and Langhoff, S.R. (1991). Theoretical study of the low-lying bound states of O_2. *J. Chem. Phys.*, **95**, 8292-8300.

[2] O'Keefe, A., and Deacon, D. A. G. (1988). Cavity ring-down optical spectrometer for absorption measurements using pulsed laser sources. *Rev. Sci. Instrum.*, **59**, 2544-2551.

[3] Bray, R.G., Henke, W., Liu, S.K., Reddy, K.V., and Berry, M.V. (1977). Measurement of highly forbidden optical transitions by intracavity CW dye laser spectroscopy. *Chem. Phys. Lett.*, **47**, 213-217.

[4] Chenevier, M., Melieres, M.A., and Stoeckel, F. (1983). Intracavity absorption line shapes and quantitative measurements on O_2. *Opt. Comm.*, **45**, 385-391.

[5] Naus, H., de Lange, A., and Ubachs, W. (1997). $b^1\Sigma_g^+$-$X^3\Sigma_g^-$ (0,0) band of oxygen isotopomers in relation to tests of the symmetrization postulate in $^{16}O_2$. *Phys. Rev. A.*, **56**, 4755-4763.

[6] Naus, H., van der Wiel, S.J., and Ubachs, W. (1998). Cavity-ring down spectroscopy on the $b^1\Sigma_g^+$-$X^3\Sigma_g^-$ (1,0) band of oxygen isotopomers. *J. Mol. Spectrosc.*, **192**, 162-168.

[7] Naus, H., Navaian, K., and Ubachs, W. (1999). The γ-band of $^{16}O_2$, $^{16}O^{17}O$, $^{17}O_2$, and $^{18}O_2$. *Spectrochim. Acta A.*, **55**, 1255-1262.

[8] Naus, H., and Ubachs, W. (1999). The $b^1\Sigma_g^+$-$X^3\Sigma_g^-$ (3,0) band of $^{16}O_2$ and $^{18}O_2$. *J. Mol. Spectrosc.*, **193**, 442-445.

[9] Biennier, L., and Campargue, A. (1998). High-resolution spectrum of the (3-0) band of the $b^1\Sigma_g^+$ - $X^3\Sigma_g^-$ red atmospheric system of oxygen. *J. Mol. Spectr.*, **188**, 248-250.

[10] Babcock, H.B., and Herzberg, L. (1948). Fine structure of the red system of atmospheric oxygen bands. *Astroph. J.*, **108**, 167-190.

[11] Brault, J. (1980). Detection of electric quadrupole transitions in the oxygen A band at 7600 Å. *J. Mol. Spectr.*, **80**, 384-387.

[12] Engeln, R., Von Helden, G., Berden, G., and Meijer, G. (1996). Phase shift cavity ring down spectroscopy. *Chem. Phys. Lett.* **262**, 105-109.

[13] Engeln, R., Berden, G., Peeters, R., and Meijer, G. (1998). Cavity-enhanced absorption and cavity enhanced magnetic rotation spectroscopy. *Rev. Sci. Instrum.*, **69**, 3763-3769.

[14] Xu, S., Dai, D., Xie, J., Sha, G., and Zhang, C. (1999). Quantitative measurements of O_2 $b \leftarrow X(2,1,0-0)$ bands by using cavity ring-down spectroscopy. *Chem. Phys. Lett.*, **303**, 171-175.

[15] Seiser, N., and Robie, D. C. (1998). Pressure broadening in the oxygen $b^1\Sigma_g^+(v'=1) \leftarrow X^3\Sigma_g^-(v"=0)$ band by cavity ring-down spectroscopy. *Chem. Phys. Lett.*, **282**, 263-267.

[16] Newman, S.M., Lane, I. C., Orr-Ewing, A. J., Newnham, D.A., and Ballard, J. (1999). Integrated absorption intensity and Einstein coefficients for the O_2 $a^1\Delta_g$-$X^3\Sigma_g^-$ (0,0) transition: A comparison of cavity ring-down and high resolution Fourier transform spectroscopy with a long path absorption cell. *J. Chem. Phys.*, **110**, 10749-10757.

[17] Miller, H.C., McCord, J.E., Choy, J, and Hager, G.D. (2001). Measurement of the radiative lifetime of O_2 ($a^1\Delta_g$) using cavity ring-down spectroscopy. *J. Quant. Spectr. Rad. Transfer*, **69**, 305-325.

[18] Jongma, R. T., Boogaarts, M. G. H., Holleman, I., and Meijer, G. (1995). Trace gas detection with cavity ring-down spectroscopy. *Rev. Sci. Instrum.*, **66**, 2821-2828.

[19] Zalicki, P., and Zare, R. N. (1995). Cavity ring-down spectroscopy for quantitative absorption experiments. *J. Chem. Phys.*, **102**, 2708-2717.

[20] Hodges, J. T., Looney, J. P., and van Zee, R. D. (1996). Laser bandwidth effects in quantitative cavity ring-down spectroscopy. *Appl. Opt.*, **35**, 4112-4116.

[21] Martin, J., Paldus, B.A., Zalicki, P. Wahl, E.H., Owano, T.G., Harris, J.S., Kruger, C.H. and Zare, R.N. (1996). Cavity ring-down spectroscopy with Fourier-transform limited pulses. *Chem. Phys. Lett.* **258**, 63-70.

[22] Huestis, D. L., Copeland, R. A., Knutsen, K., Slanger, T. G., Jongma, R. T., Boogaarts, M. G. H., and Meijer, G. (1994). Branch oscillator strengths for the Herzberg absorption systems in oxygen. *Can. J. Phys.*, **72**, 1109-1121.

[23] Slanger, T. G., Huestis, D. L., Cosby, P. C., Naus, H., and Meijer, G. (1996). O_2 photoabsorption in the 40950-41300 cm^{-1} region: New Herzberg bands, new absorption lines, and improved spectroscopic data. *J. Chem. Phys.*, **105**, 9393-9402.

[24] Yoshino, K., Esmond, J.R., Murray, J.E., Parkinson, W.H., Thorne, A.P., Learner, R.C.M., and Cox, G. (1995). Band oscillator strengths of the Herzberg I bands of O_2. *J. Chem. Phys.*, **103**, 1243-1249.

[25] Yoshino, K., Esmond, J.R., Murray, J.E., Parkinson, W.H., Thorne, A.P., Learner, R.C.M., Cox, G. and Cheung, A.S.-C. (2000). Fourier transform spectroscopy and cross section measurements of the Herzberg III bands of O_2 at 295 K. *J. Chem. Phys.*, **112**, 9791-9801.

[26] Jenouvrier, A., Mérienne, M.-F., Coquart, B., Carleer, M., Fally, S., Vandaele, A.C., Hermans, C., and Colin, R. (2000). Fourier transform spectroscopy of the O_2 Herzberg bands. *J. Mol. Spectr.*, **198**, 136-162.

[27] Naus, H., and Ubachs, W. (1999). Visible absorption bands of the $(O_2)_2$-collision complex at pressures below 760 torr. *Appl. Opt.*, **38**, 3423-3428.

[28] Newnham, D.A., and Ballard, J. (1998). Visible absorption cross sections and integrated absorption intensities of molecular oxygen (O_2 and O_4). *J. Geoph. Res. D*, **103**, 28801-28815.

[29] Biennier, L., Romanini, D., Kachanov, A., Campargue, A., Bussery-Honvault, B., and Bacis, R. (2000). Structure and rovibrational analysis of the $[O_2(a^1\Delta_g)_{v=0}]_2 \leftarrow [O_2(X^3\Sigma_g^-)_{v=0}]_2$ transition of the O_2 dimer. *J. Chem. Phys.*, **112**, 6309-6321.

[30] Berden, G., Engeln, R., Christianen, P. C. M., Maan, J. C., and Meijer, G. (1998). Cavity ring down spectroscopy on the oxygen A band in magnetic fields up to 20 Tesla. *Phys. Rev. A*, **58**, 3114-3123.

[31] Engeln, R., Berden, G., Van den Berg, E., and Meijer, G. (1997). Polarization dependent cavity ring down spectroscopy. *J. Chem. Phys.* **107**, 4458-4467.

[32] Romanini, D., Kachanov, A. A., Sadeghi, N., and Stoeckel, F. (1997). CW cavity ring down spectroscopy. *Chem. Phys. Lett.* **264**, 316-322.

[33] Peeters, R., Berden, G., Apituley, A., and Meijer, G. (2000). Open-path trace gas detection of ammonia based on cavity-enhanced absorption spectroscopy. *Appl. Phys. B*, **71**, 231-236.

[34] Berden, G., Peeters, R., and Meijer, G. (2000). Cavity ring-down spectroscopy: experimental schemes and applications. *Int. Rev. Phys. Chem.* **19**, 565-607.

[35] Gianfrani, L., Fox, R.W., and Hollberg, L. (1999). Cavity-enhanced absorption spectroscopy of molecular oxygen. *J. Opt. Soc. Am. B.*, **16**, 2247-2254.

[36] Van Zee, R. D., Hodges, J. T., and Looney, J. P. (1999). Pulsed, single-mode cavity ringdown spectroscopy. *Appl. Opt.*, **38**, 3951-3960.

[37] Meijer, G., Boogaarts, M. G. H., Jongma, R. T., Parker, D. H., and Wodtke, A. M. (1994). Coherent cavity ring down spectroscopy. *Chem. Phys. Lett.* **217**, 112-116.

[38] Romanini, D., and Lehmann, K. K. (1993). Ring-down cavity absorption spectroscopy of the very weak HCN overtone bands with six, seven, and eight stretching quanta. *J. Chem. Phys.* **99**, 6287-6301.

[39] Romanini, D., and Lehmann, K. K. (1995). Cavity ring-down overtone spectroscopy of HCN, $H^{13}CN$ and $HC^{15}N$. *J. Chem. Phys.* **102**, 633-642.

[40] Romanini, D., and Lehmann, K. K. (1996). Calculation of the Herman-Wallis effect in the Π-Σ vibrational overtone transitions in a linear molecule: comparison with HCN experimental results. *J. Chem. Phys.* **105**, 68-80.

[41] Romanini, D., and Lehmann, K. K. (1996). Line-mixing in the 106←000 overtone transition of HCN. *J. Chem. Phys.* **105**, 81-88.

[42] Campargue, A., Biennier, L., Garnache, A., Kachanov, A., Romanini, D., and Herman, M. (1999). High resolution absorption spectroscopy of the ν_1=2–6 acetylenic overtone bands of propyne: spectroscopy and dynamics. *J. Chem. Phys.* **111**, 7888-7903.

[43] Kleine, D., Stry, S., Lauterbach, J., Kleinermanns, K., and Hering, P. (1999). Measurement of the absolute intensity of the fifth CH stretching overtone of benzene using cavity ring-down spectroscopy. *Chem. Phys. Lett.* **312**, 185-190.

[44] Naus, H., Ubachs W,. Levelt, P.F., Polyanski, O.L., Zobov, N.F., and Tennyson, J. (2001). Cavity ring-down spectroscopy on water vapor in the range 555-604 nm. *J. Mol. Spectr.* **205**, 117-121.

[45] Brown, S. S., Wilson, R. W., and Ravishankara, A. R. (2000). Absolute intensities for the third and fourth overtone absorptions in HNO_3 and H_2O_2 measured by cavity ring down spectroscopy. *J. Phys. Chem. A* **104**, 4976-4983.

[46] Xu, S., Liu, Y., Sha, G., Zhang, C., and Xie, J. (2000). The O–H stretching $\Delta\nu$=3, 4, and 5 vibrational overtones and conformational study of 2-butanol. *J. Phys. Chem. A* **104**, 8671-8676.

[47] He, Y., Hippler, M., and Quack, M. (1998). High-resolution cavity ring-down absorption spectroscopy of nitrous oxide and chloroform using a near-infrared cw diode laser. *Chem. Phys. Lett.*, **289**, 527-534.

[48] O'Keefe, A., Scherer, J. J., Cooksy, A. L., Sheeks, R., Heath, J., and Saykally, R. J. (1990). Cavity ring down dye laser spectroscopy of jet-cooled metal clusters: Cu_2 and Cu_3. *Chem. Phys. Lett.*, **172**, 214-218.

[49] Yu, T., and Lin, M. C. (1993). Kinetics of phenyl radical reactions studied by the "Cavity-Ring-Down" method. *J. Am. Chem. Soc.* **115**, 4371-4372.

[50] Zalicki, P., Ma, Y., Zare, R. N., Wahl, E. H., Dadamio, J. R., Owano, T. G., and Kruger, C. H. (1995). Methyl radical measurement by cavity ring-down spectroscopy *Chem. Phys. Lett.*, **234**, 269-274.

[51] Boogaarts, M. G. H., Böcker, P.J., Kessels, W.M.M., Schram, D.C., and van de Sanden, M.C.M. (2000). Cavity ringdown detection of SiH_3 on the broadband $\tilde{A}^2A_1' \leftarrow \tilde{X}^2A_1$ transition in a remote Ar-H_2-SiH_4 plasma. *Chem. Phys. Lett.* **326**, 400-406.

[52] Booth, J. P., Cunge, G., Biennier, L., Romanini, D., and Kachanov, A. (2000). Ultraviolet cavity ring-down spectroscopy of free radicals in etching plasmas. *Chem. Phys. Lett.*, **317**, 631-636.

[53] Motylewski, T., and Linnartz, H. (1999). Cavity ring down spectroscopy on radicals in a supersonic slit nozzle discharge. *Rev. Sci. Instrum.* **70**, 1305-1312.

[54] Kotterer, M., and Maier, J. P. (1997). Electronic spectrum of C_6H: $^2\Pi - X^2\Pi$ in the gas-phase detected by cavity ringdown. *Chem. Phys. Lett.* **266**, 342-346.

[55] Spaanjaars, J. J. L., Ter Meulen, J. J., and Meijer, G. (1997). Relative predissociation rates of OH ($A^2\Sigma^+$, v'=3) from combined cavity ring down – laser induced fluorescence measurements. *J. Chem. Phys.* **107**, 2242-2248.

[56] Wheeler, M. D., Newman, S. M., Orr-Ewing, A. J., and Ashfold, M. N. R. (1998). Cavity ring-down spectroscopy. *J. Chem. Soc., Faraday Trans.* **94**, 337-351.

[57] Pearson, J., Orr-Ewing, A. J., Ashfold, M. N. R., and Dixon, R. N. (1997). Spectroscopy and predissociation dynamics of the $\tilde{A}\ ^1A''$ state of HNO. *J. Chem. Phys.* **106**, 5850-5873.

[58] Wheeler, M. D., Orr-Ewing, A. J., Ashfold, M. N. R., and Ishiwata, T. (1997). Predissociation lifetimes of the $A^2\Sigma^+$ v=1 state of the SH radical determined by cavity ring-down spectroscopy. *Chem. Phys. Lett.* **268**, 421-428.

[59] Wheeler, M. D., Orr-Ewing, A. J., and Ashfold, M. N. R. (1997). Predissociation dynamics of the $A^2\Sigma^+$ state of SH and SD. *J. Chem. Phys.* **107**, 7591-7600.

[60] Wheeler, M. D., Newman, S. M., and Orr-Ewing, A. J. (1998). Predissociation of the $B^3\Sigma_u^-$ state of S_2. *J. Chem. Phys.* **108**, 6594-6605.

[61] Wheeler, M. D., Newman, S. M., Ishiwata, T., Kawasaki, M., and Orr-Ewing, A. J. (1998). Cavity ring-down spectroscopy of the $A^2\Pi_{3/2}$ - $X^2\Pi_{3/2}$ transition of BrO. *Chem. Phys. Lett.* **285**, 346-351.

[62] Newman, S. M., Howie, W. H., Lane, I. C., Upson, M. R., and Orr-Ewing, A. J. (1998). predissociation of the $A^2\Pi_{3/2}$ state of IO studied by cavity ring down spectroscopy. *J. Chem. Soc., Faraday Trans.* **94**, 2681-2688.

[63] Howie, W. H., Lane, I. C., Newman, S. M., Johnson, D. A., and Orr-Ewing, A. J. (1999). The UV absorption of ClO- Part 1. The $A^2\Pi$ - $X^2\Pi$ spectrum at wavelengths from 285-320 nm studied by cavity ring down spectroscopy. *Phys. Chem. Chem. Phys.* **1**, 3079-3085.

[64] Ding, H., Orr-Ewing, A. J., and Dixon, R. N. (1999). Rotational structure in the $\tilde{A}^1A'' - \tilde{X}^1A'$ spectrum of formyl chloride. *Phys. Chem. Chem. Phys.* **1**, 4181-4185.

[65] Howie, W. H., Lane, I. C., and Orr-Ewing, A. J. (2000). The near ultraviolet spectrum of the FCO radical: re-assignment of transitions and predissociation of the electronically excited state. *J. Chem. Phys.* **113**, 7237-7251.

[66] Kotterer, M., Conceicao, J., and Maier, J. P. (1996). Cavity ringdown spectroscopy of molecular ions: $A^2\Pi_u \leftarrow X^2\Sigma_g^+$ (6–0) transition of N_2^+. *Chem. Phys. Lett.* **259**, 233-236.

[67] Aldener, M., Lindgren, B., Pettersson, A., and Sassenberg, U. (2000). Cavity ringdown laser absorption spectroscopy - nitrogen cation. *Physica Scripta* **61**, 62-65.

[68] Lehr, L., and Hering, P. (1997). Cavity ring-down spectroscopy of photochemically produced NaH for the determination of relative dipole transition moments. *Appl. Phys. B* **65**, 595-600.

[69] Lehr, L., and Hering, P. (1997). Quantitative nonlinear spectroscopy: a direct comparison of degenerate four-wave mixing with cavity ring-down spectroscopy applied to NaH. *IEEE J. Quantum Electron.* **33**, 1465-1473.

[70] Labazan, I., Rudić, S., and Milošević, S. (2000). Nonlinear effects in pulsed cavity ringdown spectroscopy of lithium vapor. *Chem. Phys. Lett.*, **320**, 613-622.

[71] Paul, J. B., Scherer, J. J., Collier, C. P., and Saykally, R. J. (1996). Cavity ringdown laser absorption spectroscopy and time-of-flight mass spectroscopy of jet cooled platinum silicides. *J. Chem. Phys.* **104**, 2782-2788.

[72] Scherer, J. J., Paul, J. B., Collier, C. P., O'Keefe, A., and Saykally, R. J. (1995). Cavity ringdown laser absorption spectroscopy and time-of-flight mass spectroscopy of jet-cooled gold silicides. *J. Chem. Phys.*, **103**, 9187.

[73] Scherer, J. J., Paul, J. B., Collier, C. P., and Saykally, R. J. (1995). Cavity ringdown laser absorption spectroscopy and time-of-flight mass spectroscopy of jet-cooled silver silicides. *J. Chem. Phys.* **103**, 113-120.

[74] Scherer, J. J., Paul, J. B., Collier, C. P., and Saykally, R. J. (1995). Cavity ringdown laser absorption spectroscopy and time-of-flight mass spectroscopy of jet-cooled copper silicides. *J. Chem. Phys.*, **102**, 5190.

[75] Scherer, J. J., Paul, J. B., and Saykally, R. J. (1995). Cavity ringdown laser absorption spectroscopy of the jet-cooled aluminum dimer. *Chem. Phys. Lett.* **242**, 395-400.

[76] Kraus, D., Saykally, R. J., and Bondybey, V. E. (1998). Cavity ringdown laser absorption spectra of tungsten oxide. *Chem. Phys. Lett.* **295**, 285-288.

[77] Kraus, D., Saykally, R. J., and Bondybey, V. E. (1999). Cavity ringdown spectroscopy search for transition metal dimers. *Chem. Phys.*, **247**, 431-434.

[78] Scherer, J. J., Paul, J. B., O'Keefe, A., and Saykally, R. J. (1995). CRLAS: a new analytical technique for cluster science. *Advances in Metal and Semiconductor Clusters* **3**, 149-180.

[79] Scherer, J. J., Paul, J. B., O'Keefe, A., and Saykally, R. J. (1997). Cavity ringdown laser absorption spectroscopy: history, development, and application to pulsed molecular beams. *Chem. Rev.* **97**, 25-51.

[80] Paul, J. B., Collier, C. P., Saykally, R. J., Scherer, J. J., O'Keefe, A. (1997). Direct measurement of water cluster concentrations by infrared cavity ringdown laser absorption spectroscopy. *J. Phys. Chem. A* **101**, 5211-5214.

[81] Provencal, R. A., Paul, J. B., Roth, K., Chapo, C., Caseas, R. N., Saykally, R. J., Tschumper, G. S., and Schaeffer III, H. F. (1999) Infrared cavity ringdown spectroscopy of methanol clusters: Single donor hydrogen bonding. *J. Chem. Phys.*, **110**, 4258-4267.

[82] Provencal, R. A., Casaes, R. N., Roth, K., Paul, J. B., Chapo, C. N., Saykally, R. J., Tschumper, G. S., and Schaefer III, H. F. (2000). Hydrogen bonding in alcohol clusters: a comparative study by infrared cavity ringdown laser absorption spectroscopy. *J. Phys. Chem. A.* **104**, 1423-1429.

[83] Paul, J. B., Provencal, R. A., Chapo, C., Roth, K., Casaes, R., and Saykally, R. J. (1999). Infrared cavity ringdown spectroscopy of water cluster bending vibrations. *J. Phys. Chem. A* **103**, 2972-2974.

[84] Chapo, C. J., Paul, J. B., Provencal, R. A., Roth, K., and Saykally, R. J. (1998) Is arginine zwitterionic or neutral in the gas phase? Results from IR cavity ringdown spectroscopy. *J. Am. Chem. Soc.* **120**, 12956-12957.

[85] Boogaarts, M. G. H., and Meijer, G. (1995). Measurement of the beam intensity in a laser desorption jet-cooling mass spectrometer. *J. Chem. Phys.* **103**, 5269-5274.

[86] Ruth, A. A., Fernholz, T., Brint, R. P., and Mansfield, M. W. D. (1998). The cavity ring-down absorption spectrum of the $S_0 \rightarrow T_1$ and $S_0 \rightarrow S_1$ transition of jet-cooled 4-H-1-benzopyrane-4-thione. *Chem. Phys. Lett.* **287**, 403-411.

[87] Ruth, A. A., Kim, E. K., and Hese, A. (1999). The $S_0 \rightarrow S_1$ cavity ring-down absorption spectrum of jet-cooled azulene: dependence of internal conversion on excess energy. *Phys. Chem. Chem. Phys.* **1**, 5121-5128.

[88] Romanini, D., Biennier, L., Salama, F., Kachanov, A., Allamandola, L. J., and Stoeckel, F. (1999). Jet-discharge cavity ring-down spectroscopy of ionized polycyclic aromatic hydrocarbons: progress in testing the PAH hypothesis for the diffuse interstellar band problem. *Chem. Phys. Lett.* **303**, 165-170.

[89] Linnartz, H., Motylewski, T., Vaizert, O., Maier, J. P., Apponi, A. J., McCarthy, M. C., Gottlieb, C. A., and Thaddeus, P. (1999). Electronic ground and excited state spectroscopy of C_6H and C_6D. *J. Mol. Spectrosc.* **197**, 1-11.

[90] Linnartz, H., Motylewski, T., and Maier, J. P. (1998). The $^2\Pi \leftarrow X^2\Pi$ electronic spectra of C_8H and $C_{10}H$ in the gas phase. *J. Chem. Phys.* **109**, 3819-3823.

[91] Pfluger, D., Motylewski, T., Linnartz, H., Sinclair, W. E., and Maier, J. P. (2000). Rotationally resolved $A^2\Pi_u \leftarrow X^2\Pi_g$ electronic spectrum of tetra-acetylene cation. *Chem. Phys. Lett.* **329**, 29-35.

[92] Linnartz, H., Vaizert, O., Motylewski, T., and Maier, J. P. (2000). The $X^3\Sigma_u^- \leftarrow X^3\Sigma_g^-$ electronic spectrum of linear C_4 in the gas phase. *J. Chem. Phys.* **112**, 9777-9779.

[93] Motylewski, T., Vaizert, O., Giesen, T. F., Linnartz, H., and Maier, J. P. (1999). The $^1\Pi_u \leftarrow X^1\Sigma_g^+$ electronic spectrum of C_5 in the gas phase. *J. Chem. Phys.* **111**, 6161-6163.

[94] Vaizert, O., Motylewski, T., Wyss, M., Riaplov, E., Linnartz, H., and Maier, J.P. (2001). The $A^3\Sigma^-$ - $X^3\Sigma^-$ electronic transition of HC_6N. *J. Chem. Phys.* **114**, 7918-7922.

[95] Motylewski, Linnartz, H., T., Vaizert, O., Maier, J. P., Galazutdinov, G.A., Musaev, F.A., Krelowski, J., Walker, G.A.H., and Bohlender, D.A. (2000). *Astroph. J.* **531**, 312-320.

[96] Ball, C. D., McCarthy, M. C., and Thaddeus, P. (1999). Laser spectroscopy of the carbon chains HC_7H and HC_9H. *Astrophys. J.* **523**, L89-L91.

[97] Ball, C. D., McCarthy, M. C., and Thaddeus, P. (2000). Cavity ringdown spectroscopy of the linear carbon chains HC_7H, HC_9H, $HC_{11}H$, and $HC_{13}H$. *J. Chem. Phys.* **112**, 10149-10155.

[98] Moule, D. C., Burling, I. R., Liu, H., and Lim, E. C. (1999). The cavity ringdown spectrum of the visible electronic system of thiophosgene: an estimation of the lifetime of the $T_1(\tilde{a}^3A_2)$ triplet state. *J. Chem. Phys.*, **111**, 5027-5037.

[99] Paulisse, K. W., Friday, T. O., Graske, M. L., and Polik, W. (2000). Vibronic spectroscopy and lifetime of S_1 acrolein. *J. Chem. Phys.* **113**, 184-191.

[100] Müller, T., Vaccaro, P. H., Pérez-Bernal, F., and Iachello, F. (2000). Algebraic approach for the calculation of polyatomic Franck-Condon factors: application to the vibronically resolved absorption spectrum of disulfur monoxide (S_2O). *Chem. Phys. Lett.* **329**, 271-282.

[101] Liu, K., Dulligan, M., Bezel, I., Kolessov, A., and Wittig, C. (1998). Quenching of interconversion tunneling: the free HCl stretch first overtone of $(HCl)_2$. *J. Chem. Phys.* **108**, 9614-9616.

[102] Ito, F., and Nakanaga, T. (2000). A jet-cooled infrared spectrum of the formic acid dimer by cavity ring-down spectroscopy. *Chem. Phys. Lett.* **318**, 571-577.

[103] Romanini, D., Dupré, P., and Jost, R. (1999). Non-linear effects by continuous wave cavity ringdown spectroscopy in jet-cooled NO_2. *Vibr. Spectrosc.* **19**, 93-106.

[104] Hippler, M., and Quack, M. (1999). CW cavity ring-down infrared absorption spectroscopy in pulsed supersonic jets: nitrous oxide and methane. *Chem. Phys. Lett.* **314**, 273-281.

[105] Naus, H., and Ubachs, W. (2000). Experimental verification of Rayleigh-scattering cross sections. *Opt. Lett.*, **25**, 347-349.

[106] Lewis, E. K., Reynolds, D., Li, X., De Villele, G., Leduc, C., Cedeño, D. L., Manzanares I, C. (2001). Phase shift cavity ring-down measurement of C–H (Δv=6) vibrational overtone absorptions. *Chem. Phys. Lett.* **334**, 357-364.

[107] Berden, G., Peeters, R., and Meijer, G. (1999) Cavity-enhanced absorption spectroscopy of the 1.5 μm band system of jet-cooled ammonia. *Chem. Phys. Lett.*, **307**, 131-138.

[108] Peeters, R., Berden, G., and Meijer, G. (2001) Near-infrared cavity enhanced absorption spectroscopy of hot water and OH in an oven and flames. *Appl. Phys. B*, **73**, 65-70.

[109] Müller, T., Wiberg, K.B., and Vaccaro P.H. (2000). Cavity ring-down polarimetry (CRDP): a new scheme for probing circular birefringence and circular dichroism in the gas phase. *J. Phys. Chem. A* **104**, 5959-5968.